



Article

Ionospheric Peak Parameters Retrieved from FY-3C Radio Occultation: A Statistical Comparison with Measurements from COSMIC RO and Digisondes Over the Globe

Han Wang ¹, Jia Luo ^{1,2,*}  and Xiaohua Xu ^{1,3} 

¹ School of Geodesy and Geomatics, Wuhan University, 129 Luoyu Road, Wuhan 430079, China; 2013301610012@whu.edu.cn (H.W.); xhxu@sgg.whu.edu.cn (X.X.)

² Key Laboratory of Geospace Environment and Geodesy, Ministry of Education, 129 Luoyu Road, Wuhan 430079, China

³ Collaborative Innovation Center for Geospatial Technology, 129 Luoyu Road, Wuhan 430079, China

* Correspondence: jialuo@whu.edu.cn; Tel.: +86-27-68778531

Received: 29 March 2019; Accepted: 12 June 2019; Published: 14 June 2019



Abstract: In this study, two ionospheric peak parameters (ICPs), NmF2 and hmF2, derived from the global navigation satellite system (GNSS) radio occultation (RO) ionospheric electron density profiles (EDPs) obtained by Feng-Yun 3C (FY-3C) mission are compared with those derived from the observations of the Constellation Observing System for the Meteorology, Ionosphere, and Climate (COSMIC) mission and the measurements from 24 digisonde stations distributed around the world during the year from 2014 to 2017. The FY-3C derived ICPs and the COSMIC-derived ICPs are provided by the National Satellite Meteorological Centre (NSMC) and the COSMIC Data Analysis and Archive Center (CDAAC), respectively. The correlation and bias analyses are carried out in the comparison under the collocation criterion with the time interval of 1 h and the space interval of 3° in latitude and 5° in longitude. When comparing the ICPs derived from the two RO missions, the difference in the azimuth of occultation planes (DAOPs) between the matched pairs is limited to be within 20°. The comparison results are analyzed for different solar activity periods, and solar elevation angle (SEA) is taken for the first time as a factor that represents the comprehensive impacts of latitude zones, seasons, and local time of the observations. The results are shown as follows: (1) Both the COSMIC RO-derived and the digisonde-observed ICPs are in good agreement with the FY-3C RO-derived ones. The correlation coefficient (CC) between the NmF2 and hmF2 derived by COSMIC RO and FY-3C RO is 0.965 and 0.916, respectively, while the correlation coefficient between the NmF2 and hmF2 derived by digisonde and FY-3C RO is 0.924 and 0.832, respectively. The quality of FY-3C RO-derived ICPs are reliable enough for further applications. (2) The CC of NmF2 is, in general, higher than that of hmF2 when comparing FY-3C RO with other observations, and the overall MAB and MRB of FY-3C RO-derived ICPs during the higher solar activity period are higher than the ones during the lower solar activity period. The difference between the two RO missions is much smaller than that one between FY-3C RO and digisonde. (3) For a certain solar activity period, the standard deviations of the absolute bias (SDAB) and the standard deviations of the relative bias (SDRB) of FY-3C RO-derived ICPs compared with digisonde-derived ones generally increases with the increase of SEA, while the SDAB and SDRB of FY-3C RO-derived ICPs both get the minimum values for the AOP interval near to 90°.

Keywords: radio occultation; FY-3C; COSMIC; digisonde; correlation; bias; solar elevation angle

1. Introduction

In recent years, the global navigation satellite system (GNSS) radio occultation (RO) has become an essential modern technique for observing the Earth's atmosphere [1–3]. One important application of GNSS RO is ionosphere monitoring [4–6]. The electron density profiles (EDPs) provided by RO with high vertical resolution and global coverage are useful supplements to the observations from traditional ionospheric probing techniques such as incoherent scatter radar and digisonde. Since the 1960s, more than 20 low Earth orbit (LEO) satellites equipped with GNSS RO receivers have been launched, including the Challenging Minisatellite Payload (CHAMP) [7], the Gravity Recovery and Climate Experiment (GRACE) [8], the Constellation Observing System for the Meteorology, Ionosphere, and Climate (COSMIC) [9], MetOp-A, MetOp-B [10], Feng-Yun 3C (FY-3C) [11,12], and so on. The observation data provided by these GNSS RO missions contribute much to space environment monitoring [6,13] and were applied in ionospheric climate studies [14–16].

The FY-3C satellite, which was launched in September of 2013 and finally operates in the orbit of 836 km altitude and 98.75° inclination, is able to track the occultation signals of both GPS and BDS simultaneously [12,17–19]. The FY-3C RO ionospheric products, including the time and location of the RO events and the corresponding electron density profiles (EDPs), have been provided by the National Satellite Meteorological Centre (NSMC) since 2014, whose quality has been validated in some comparisons with the observations from COSMIC RO mission and digisondes [12,19]. COSMIC is the first LEO constellation designed for GNSS RO observations, which has provided more than two million EDPs since it was launched in 2006 [3,6], while digisonde is the traditional technique for measuring the ionosphere status below the peak heights with high accuracy and reliability [20–22]. Meanwhile, the most significant error source of RO-derived EDPs is the assumption of the spherical symmetry of the atmospheric refractive index in the inversion process, which means that it is assumed that there is no horizontal gradient of electron density around the spherical shell [23,24]. Therefore, the performance of RO ionospheric products would degrade where large horizontal electron density gradient exists or when severe ionospheric fluctuation occurs [25].

In most previous studies on the validation and the application of the FY-3C RO ionospheric products, the time periods concerned about are generally not longer than one year. For example, Mao et al. [12] validated the FY-3C RO EDPs for 92 days in 2013, from day of year (DOY) 274 to DOY 365, while Yang et al. [19] studied the quality of FY-3C RO ionospheric characteristic parameters (ICPs) during the time period of only one year from October 1, 2013 to September 30, 2014. Yang et al. [26] used the RO-derived EDPs provided by FY-3C from June 2014 to May 2015 to study the disturbance strength of sporadic E layers. Although it is concluded by Yang et al. [26] that the EDPs derived from FY-3C RO are applicable for ionospheric physics studies, the validation based on long-term data is needed to make this argument more convincing. In addition, FY-3C EDPs provided by NSMC are retrieved using the standard Abel inversion [12], which results in that the occultation direction would have an impact on the quality of the RO products. There is still no validation work on FY-3C RO ionospheric parameters which takes into consideration the occultation direction of RO planes.

Furthermore, in previous studies about the validation of ionospheric products from CHAMP [27], COSMIC [28–31], FY-3C [12,19], and other RO missions [5] with digisonde measurements, when analyzing the variation of the quality of RO ionospheric parameters with different impact factors, the factors taken into consideration generally include latitude, season, and local time of the observation. For example, the comparison of FY-3C RO EDPs and digisonde-derived ones carried out by Yang et al. [19] focused on the performance of FY-3C RO ICPs over different latitude regions and during daytime/night-time. Considering that the variations of these factors are not independent in the temporal and distribution of RO events, it is difficult to get a general conclusion on the impact of a certain factor on RO-derived ionospheric parameters. For example, the variation of the latitudes of RO events makes the analysis complicated when it is aimed to study the variation of the quality of RO-derived ICPs with seasons. Therefore, when comparing the ionospheric products derived from FY-3C RO with other independent observations, to introduce a new factor that integrates the impacts

of latitude, season, and local time would be helpful to simplify the analysis of the comparison results and to get constructive conclusions.

In this study, to validate the quality of FY-3C RO ionospheric products, we compared the ICPs derived from FY-3C RO with those from COSMIC RO and 24 digisondes, which are distributed globally. The comparison is carried out during the four years from 2014 to 2017, which is much longer than the time periods concerned about in previous studies. The direction of each RO plane, which is denoted by the azimuth of the occultation plane (AOP), is taken into consideration in the validation. When analyzing the variation pattern of the quality of FY-3C RO-derived ICPs, the solar elevation angle (SEA) is used as an integrated factor replacing the three factors traditionally used, including latitude zone, season, and local time.

In addition, because the quality of RO-inverted ionospheric parameters is influenced by the geomagnetic conditions and the solar activity level, these two factors are also taken into consideration in the comparison. F10.7 index, i.e., the solar radio flux at 10.7 cm (2800 MHz), which is an excellent indicator for the level of solar activity, and Ap (the equivalent planetary daily amplitude) index, which is used to identify different geomagnetic conditions, are both downloaded from NASA's Space Physics Data Facility (SPDF; <https://omniweb.gsfc.nasa.gov/form/dx1.html>) and are shown in Figure 1. According to Figure 1a, the period of 2014–2015 and the period of 2016–2017 is classified as the higher solar activity period and the lower solar activity period, respectively. While according to Figure 1b, the observations that were obtained during geomagnetically disturbed periods (i.e., $A_p > 12$) will not be considered in this study [32].

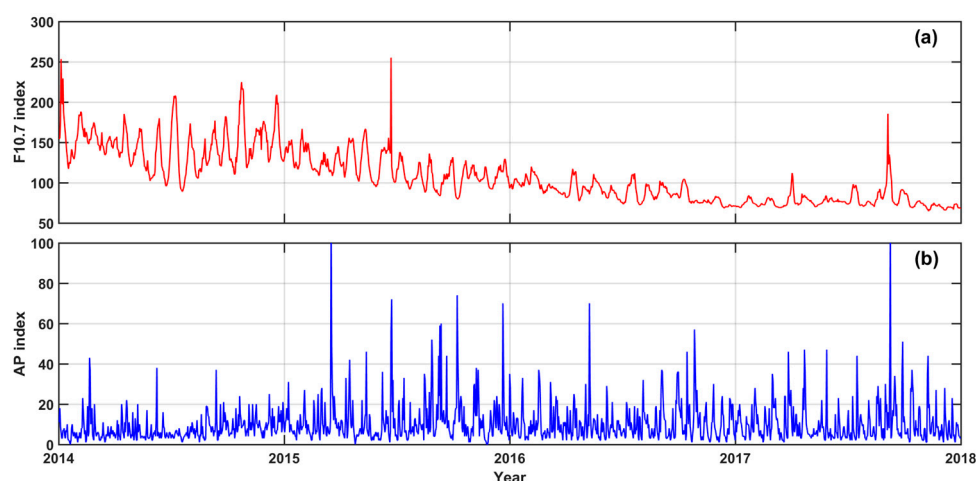


Figure 1. Variations of daily F10.7 index (a) red line and Ap (the equivalent planetary daily amplitude) index (b) blue line during the year from 2014 to 2017.

Data and method are introduced in Section 2 and the results are presented in Section 3. In Section 4, the possible principles to explain the results are discussed and the conclusions are drawn in Section 5.

2. Data and Methods

2.1. RO Data

FY-3C RO EDP data were obtained from the “EDP” files provided by NSMC (<http://satellite.nsmc.org.cn>), and COSMIC RO EDP data were obtained from the “ionPrf” files provided by CDAAC (<http://cdaac-www.cosmic.ucar.edu>). The post-processed EDPs from the two RO missions during the time period from 2014 to 2017 were used to conduct the long-term statistical comparisons. Although some other advanced inversion algorithms have been brought forward [25,33–35], both the COSMIC EDPs in “ionPrf” files provided by CDAAC and the FY-3C EDPs provided by NSMC were obtained based on GPS L1 and L2 phase observations by using the standard Abel inversion [12,25,36]. It is

important to note that the assumption of a spherically symmetric ionosphere in the Abel inversion might introduce systematic errors in the retrieved electron density [23].

In addition, due to the random fluctuations and steep gradients of the plasma density along the GPS ray path, the influences of observation errors and the approximations used in the inversion process, gross errors may exist in the inverted EDPs [37]. It was found that some questionable EDPs, e.g., some EDPs with exceedingly irregular fluctuations in the height variations of electron densities and some EDPs with positive topside gradients, exist in the downloaded COSMIC-RO and FY-3C RO products [19,38]. In this work, the qualities of FY-3C and COSMIC RO EDPs are checked using the criteria applied in the references [37–39], which are summarized in Table 1 [40].

Table 1. Radio occultation (RO)-derived electron density profile (EDP) quality control criteria [40].

Quality Control Parameter	Formula or Sources	Qualified Condition	Note
MD	$MD = \sum_{i=1}^N \frac{ n_e(i) - \bar{n}_e(i) }{N \cdot n_e(i)}$	MD < 0.1	
δ	$\delta = \sqrt{\frac{\sum_{i=1}^N (n_e(i) - \bar{n}_e(i))^2}{N \cdot (N_m F_2)^2}}$	$\delta < 0.05$	
∇_g	$\nabla_g = \frac{dn_e}{dh}$	$\nabla_g < 0$	$h \geq h_m F_2$
∇_l	$\nabla_l = \frac{dn_e}{dh}$	$\nabla_l < 0$	$420 \text{ km} \leq h \leq 490 \text{ km}$
$N_m F_2$	Given in the EDP files	$h_m F_2 \geq 0$	
$h_m F_2$	Given in the EDP files	$N_m F_2 \geq 200 \text{ km}$	

In Table 1, the quality control parameters, the formula used to calculate these parameters or the sources to get them, and the corresponding qualified conditions are listed in the first three columns. Among the six quality control parameters, the parameter MD, which means the mean relative deviation of an EDP, and the parameter δ , which denotes the noise factor of an EDP, were both calculated based on the total number of the data points in the EDP, N , and the measured and the smoothed electron density at the i th data point ($n_e(i)$ and $\bar{n}_e(i)$ ($i = 1, 2, \dots, N$)); the parameter ∇_g , which means the global topside gradient, and the parameter ∇_l , which means the local topside gradient, were both calculated using the measured electron densities n_e at a specified height range denoted in the fourth column; while the other two parameters, the peak density $N_m F_2$ and the peak height $h_m F_2$ were both given directly in the EDP files.

Figure 2 shows the numbers and the percentages of the RO EDPs before and after the Ap index check and further after quality control during each year and during the whole time period. For the whole time period, the percentage of FY-3C and COSMIC RO EDPs, which were used in the present analyses, was 42.3% and 54.6%, respectively, and this percentage varies from year to year. It can be seen from Figure 2b that although COSMIC could provide up to 2500 daily EDPs at the early stages of its operation [3,6], the number of profiles declined greatly during 2014 to 2017 due to the aging and loss of the satellites.

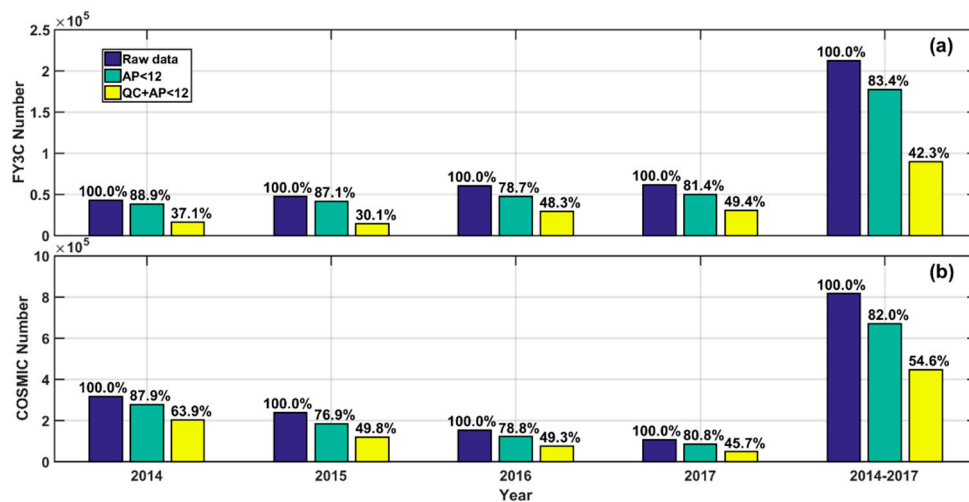


Figure 2. Variations of the numbers and the percentage of RO electron density profiles before and after the Ap index check and further after quality control for (a) Feng-Yun 3C (FY-3C); and (b) the Constellation Observing System for the Meteorology, Ionosphere, and Climate (COSMIC).

Except for the EDPs of the two RO missions, we also need the AOP corresponding to each qualified RO EDP. The AOPs of COSMIC EDPs were available in the “ionPrf” files provided by CDAAC, while the AOPs of FY-3C RO planes were not presented in the NSMC dataset. We calculated the AOP of each FY-3C RO plane using the information of the satellite positions during the ROE, which was presented in the “IEG” files provided by NSMC. What needs to be mentioned is that the AOP is defined as the azimuth at the tangent point of the ray path with respect to the north direction, and the original azimuth angles varied in the range $(-180^\circ, 180^\circ)$. In the present study, following Shaikh et al. [24], AOP was reduced to the range of $(0^\circ, 180^\circ)$ considering that for the same location, two occultation directions with the azimuth angle difference of 180° were actually on the same line of ray path. Figure 3 shows the distributions of the AOPs corresponding to all the qualified FY-3C and COSMIC EDPs during the studied time period. The distributions of the AOPs corresponding to the qualified EDPs that are collocated with digisonde observations are also shown in this figure. It can be seen that the distribution patterns of the AOPs of qualified RO EDPs from the two RO missions were similar. The percentage of the AOPs in the range of 50° – 130° was smaller than that of the AOPs in the other range of 0° – 180° . After being collocated with digisonde observations, this feature in the distribution patterns of the AOPs of RO EDPs was also kept.

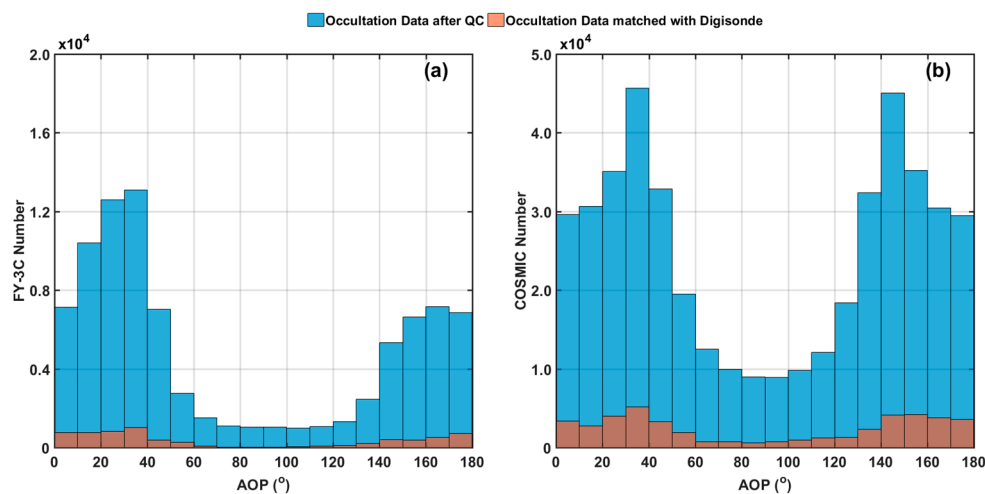


Figure 3. Distributions of the azimuth of the occultation planes (AOPs) of the qualified RO EDPs and of the RO EDPs collocated with digisonde observations for (a) FY-3C and (b) COSMIC.

2.2. Digisonde Data

The ICPs observed by 24 globally distributed digisonde stations, which were provided by the Global Ionospheric Radio Observatory (GIRO) and were available via the Digital Ionogram DataBase (DIDB, <http://ulcar.uml.edu/DIDBase/>), were used in this study for the comparison with FY-3C RO measurements. The locations of the 24 digisonde stations are shown in Figure 4. What needs to be mentioned is that these ICPs were auto-scaled using an automatic real-time ionogram scaler with true height (ARTIST)-4/5 [21,41]. To minimize the uncertainties arising due to autoscaling and to maintain the accuracy, we followed Kumar et al. [41] by using the confidence score (CS) of these auto-scaled data, which is based on a system of quality criteria interspersed within the logic and algorithm of the ionogram interpretation, as well as certain “sanity” checks applied to the autoscaling outcome [42]. The values of CS vary from 0 to 100, and a higher value corresponds to a better confidence level. In the present study, to ensure that all the digisonde-derived ICPs used in the analysis were of the best confidence level, we only used those ICPs with CS equal to 100. The sampling frequencies of the digisonde stations varied from 5 min to 15 min, and most of them are of the frequencies of 15 min. The number of the digisonde ICPs passing through the quality check during the studied time period is 958041, which was 23.3% of the total number of 4104005 digisonde ICPs analyzed.

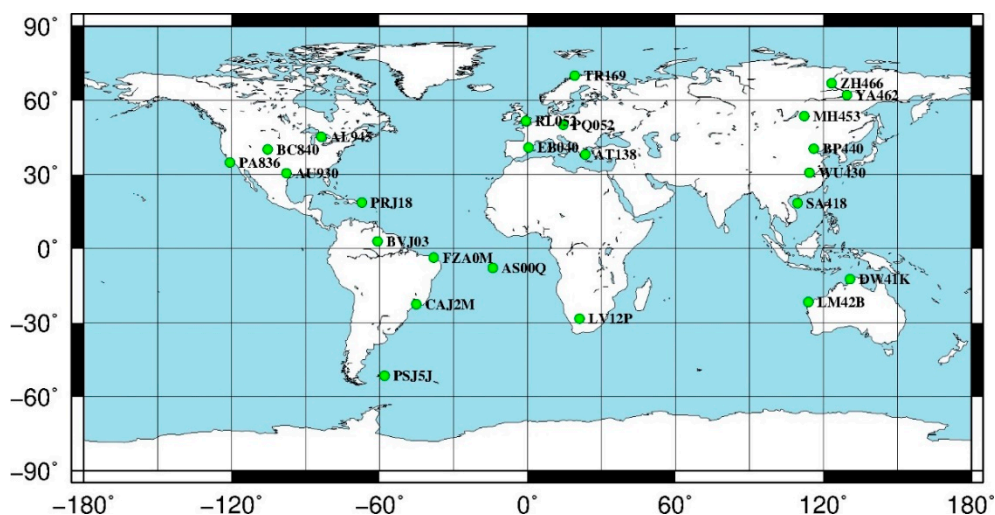


Figure 4. The distribution of the 24 digisonde stations.

2.3. Statistical Method

When comparing the observations from FY-3C RO with COSMIC RO and digisonde observations, matched observation pairs of FY-3C RO and COSMIC RO (digisonde) should be obtained under certain collocation criteria. In this work, we used the space and time collocation windows of (3°, 5°, 1 h), which means that if the tangent point at the F2 peak height of a FY-3C RO observation lies within 3° in latitude and 5° in longitude of the F2 peak height of a COSMIC RO observation or the location of a given digisonde station, with a time difference between the two observations of less than 1 h, then the two observations were considered as one matched pair. The space window used here was consistent with which was used by [43], and the different separations of latitude window and longitude window were consistent with NmF2 being better correlated in the east-west direction than in the north-south direction [44]. The time window of 1 h was used by [45] for comparing COSMIC RO-derived ICPs with digisonde-derived ones. Furthermore, according to our analyses about the influence of the collocation windows on the comparisons of the ICPs derived from RO and digisondes [40], there can be appropriate relaxation on the time window within the threshold of 1 h to get a balance between the quality of the comparison results and the number of the matched pairs.

As mentioned in Section 2.1, systematic errors may exist in the FY-3C and COSMIC RO EDPs retrieved with Abel inversion because of the assumption of spherically symmetric ionosphere. For a pair of RO EDPs collocated in space and time, the systematic errors introduced by the inversion method will be similar and will be cancelled in the comparison if the two occultation directions are close to each other. Therefore, when comparing the ICPs derived from the two RO missions, it is compulsory to set a constraint on the difference in the occultation directions of the matched pairs. This constraint will help to eliminate the difference in the effects of the spherical symmetry assumption on the matched RO-inverted ICPs and make the comparison more convinced. The corresponding comparison results would demonstrate the inherent quality differences between the two RO missions. In the present work, this constraint is set as that the difference in the AOP (DAOP) of the collocated pairs should be less than 20° .

ICPs were extracted from the data files of collocated FY-3C RO and COSMIC RO (digisonde) EDPs, based on which several statistical parameters were calculated, including the correlation coefficients (CCs) between FY-3C RO-derived and COSMIC RO-derived (digisonde-derived) ICPs and the biases of FY-3C-derived ICPs compared with the COSMIC RO-derived (digisonde-derived) ones. The correlation coefficient (R) is defined by Equation (1). The mean absolute bias (MAB) and the mean relative bias (MRB) is defined by the Equations (2) and (3), respectively. While the corresponding standard deviation of the absolute bias (SDAB) and the standard deviation of the relative bias (SDRB) is defined by the Equations (4) and (5), respectively.

$$R = \frac{\sum_{i=1}^N (IPP_i^O - \frac{1}{N} \sum_{i=1}^N IPP_i^O) \cdot \sum_{i=1}^N (IPP_i^F - \frac{1}{N} \sum_{i=1}^N IPP_i^F)}{\sqrt{\sum_{i=1}^N (IPP_i^O - \frac{1}{N} \sum_{i=1}^N IPP_i^O)^2} \sqrt{\sum_{i=1}^N (IPP_i^F - \frac{1}{N} \sum_{i=1}^N IPP_i^F)^2}}, \quad (1)$$

$$MAB = \frac{1}{N} \sum_{i=1}^n (ICP_i^F - ICP_i^O), \quad (2)$$

$$MRB = \frac{1}{N} \sum_{i=1}^n \left(\frac{ICP_i^F - ICP_i^O}{ICP_i^O} \right), \quad (3)$$

$$SDAB = \sqrt{\frac{1}{N} \sum_{i=1}^n (ICP_i^F - ICP_i^O - MAB)^2}, \quad (4)$$

$$SDRB = \sqrt{\frac{1}{N} \sum_{i=1}^n \left(\frac{ICP_i^F - ICP_i^O}{ICP_i^O} - MRB \right)^2}, \quad (5)$$

where ICP^F and ICP^O represents the ICP value from FY-3C RO and the other observation (COSMIC RO or digisonde), respectively. The subscript i represents the i -th collocated pairs, and N is the total number of collocated pairs. R represents the correlation between FY-3C RO-derived and COSMIC RO-derived (digisonde-derived) ICPs, and larger value of R corresponds to a better agreement between the matched observations. Here, the biases of FY-3C RO-derived ICPs compared with the ICPs derived from digisondes are used to evaluate the performance of FY-3C RO ionospheric products because digisonde observations are generally of high accuracy and can be used as independent references to validate the RO measurements [28–31]. The biases of FY-3C RO-derived ICPs compared with COSMIC RO-derived ones are obtained to understand the degree of consistency between the measurements from the two different RO missions.

3. Results and Analyses

3.1. The Correlations and Biases between the ICPs Derived from FY-3C RO and Other Observations

During the four years from 2014 to 2017, 2661 pairs of FY-3C RO-derived and COSMIC RO-derived EDPs were obtained under the space and time collocation windows of (3° , 5° , 1 h). While only 935 pairs of them were of DAOPs less than 20° . The comparison results of these 2661 data pairs and 935 data pairs are shown in Figures 5 and 6, respectively. During the four years, 6576 pairs of FY-3C RO-derived and digisonde derived EDPs were obtained under the space and time collocation windows of (3° , 5° , 1 h). The distribution of AOPs of FY-3C RO in these data pairs is shown in Figure 3a. It can be seen that most of the AOP values were out of the range of 50° – 130° . The comparison results of these 6576 data pairs are shown in Figure 7. In each of these three figures, the scatter plots of the data pairs (Figures 5a,d, 6a,d and 7a,d), the distribution of the absolute biases (ABs; Figures 5b,e, 6b,e and 7b,e) and that of the relative biases (RBs; Figures 5c,f, 6c,f and 7c,f) are presented. The upper subgraphs and the lower subgraphs represent the comparison results of NmF2 and hmF2, respectively. In the subfigures (Figures 5a,d, 6a,d and 7a,d), the red dots and the black lines represent the data pairs and the $y = x$ reference lines, respectively, while the numbers of the matched couples, the CCs, the equations of the regression lines are given by the notes. In the subfigures (Figures 5b,c, 6b,c and 7b,c) and (Figures 5e,f, 6e,f and 7e,f), the blue columns and the red curves represent the probabilities corresponding to certain bias intervals and the fit lines of the cumulative distribution of the probability (CDF), respectively, while the statistical comparison parameters and the proportions of specified bias intervals are given by the notes.

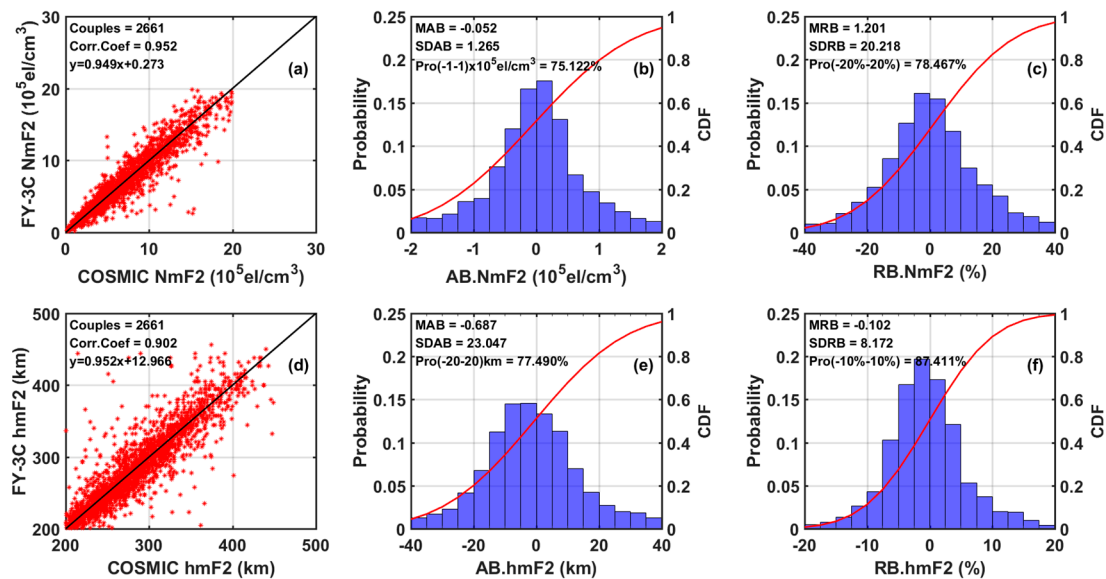


Figure 5. The comparison of FY-3C RO-derived ionospheric characteristic parameters (ICPs) with ICPs derived from COSMIC RO during 2014–2017 based on the collocation space and time windows of (3° , 5° , 1 h) for the statistical parameters of (a,d) correlation coefficients, (b,e) absolute biases, and (c,f) relative biases.

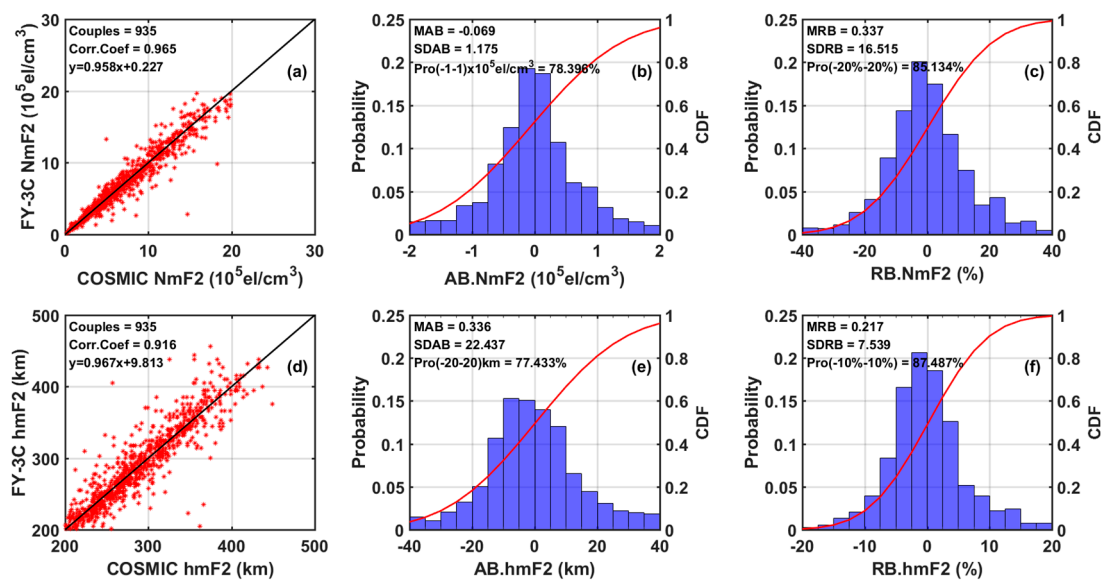


Figure 6. The comparison of FY-3C RO-derived ICPs with ICPs derived from COSMIC RO during 2014–2017 based on the collocation space and time windows of (3° , 5° , 1 h) and the constraint of $DAOP \leq 20^\circ$ for the statistical parameters of (a,d) correlation coefficients, (b,e) absolute biases, and (c,f) relative biases.

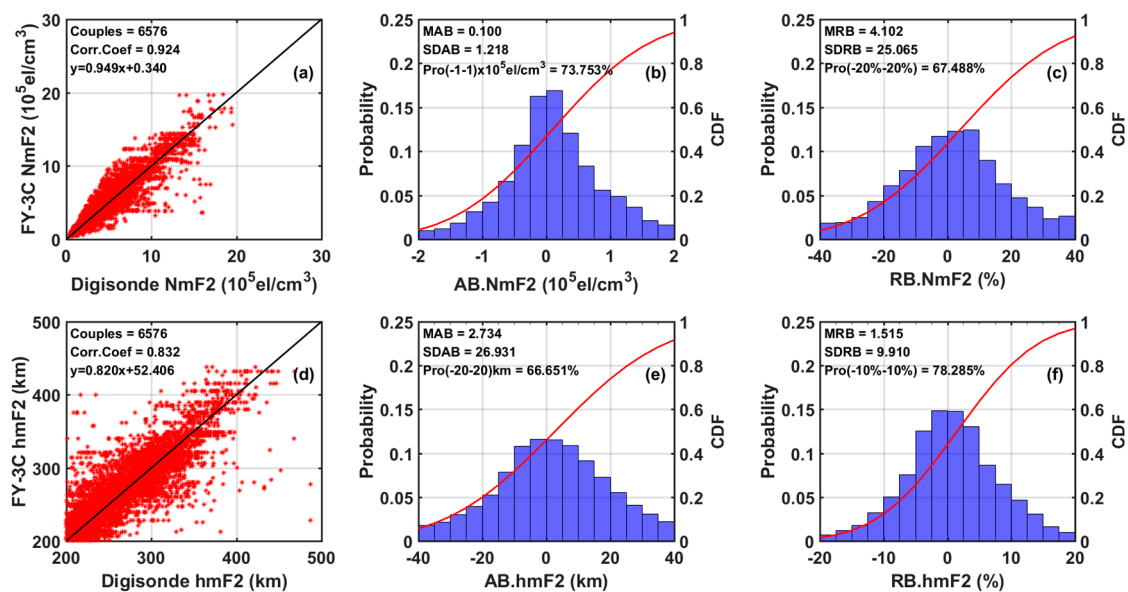


Figure 7. The comparison of FY-3C RO-derived ICPs with ICPs derived from digisonde during 2014–2017 based on the collocation space and time windows of (3° , 5° , 1 h) for the statistical parameters of (a,d) correlation coefficients, (b,e) absolute biases, and (c,f) relative biases.

From Figures 5a,d and 6a,d, it can be seen that for the comparison between FY-3C RO-derived ICPs and COSMIC RO-derived ones, no matter whether the constraint on DAOP was set in the collocation criteria or not, the slopes of the regression lines of NmF2 and hmF2 were both close to 1, and the CC of NmF2 and that of hmF2 were both greater than 0.9, while the former was a little higher than the latter. Figure 6b,c present that with COSMIC RO-derived ICPs as references, the proportion of FY-3C NmF2 values, which were of ABs (RBs) with absolute values less than 1×10^5 el/cm³ (20%) was 78.396% (85.134%) when the constraint on DAOP was applied, which was of a lower value when there was no constraint on DAOP, as shown in Figures 5b,c, 5e,f and 6e,f reveals that with COSMIC RO-derived ICPs as references, the proportion of FY-3C hmF2 that were of ABs (RBs) with absolute values less than

20 km (10%) decreased (increase) a little when the constraint on DAOP was set compared with when there was no constraint on DAOP.

Figure 7a,d presents that for the comparison between FY-3C RO-derived ICPs and digisonde-derived ones, the correlation of NmF2 was also higher than that of hmF2. Figure 7b,c,e,f shows that with digisonde-derived ICPs as references, the proportion of FY-3C NmF2 values that were of ABs (RBs) with absolute values less than 1×10^5 el/cm³ (20%) was 73.753% (67.488%), while the proportion of FY-3C hmF2 values that were of ABs (RBs) with absolute values less than 20 km (10%) was 66.651% (78.285%). These proportion values were generally lower than the corresponding ones shown in Figures 5 and 6.

The statistical comparison parameters, including CC, MAB, MRB, SDAB, and SDRB, which are presented in Figures 5–7 and are summarized in Table 2. As shown in this table, there was good agreement between FY-3C RO and other observations (COSMIC RO or digisonde) in the four years. To be specific, the correlations between FY-3C RO-derived ICPs and COSMIC RO-derived (digisonde-derived) ICPs were all higher than 0.92 (0.83). Meanwhile, the correlation of NmF2 was better than that of hmF2 for each of the three comparison schemes. Furthermore, no matter whether the constraint on DAOP was set for the collocation of RO-derived ICPs or not, the CC (MAB, MRB, SAB, SRB) between FY-3C RO-derived ICPs and COSMIC RO-derived ICPs was generally higher (lower) than that between FY-3C RO-derived ICPs and digisonde-derived ICPs. It indicates that compared with the ICPs derived from digisondes, the FY-3C RO-derived ICPs were more consistent with those derived from COSMIC RO. It could be attributed to that the standard Abel inversion method used to retrieve RO EDPs introduced systematic errors in the ICPs from both of the two RO missions, while digisonde-derived ICPs were not affected by this error source. The inconsistency revealed by the comparison of FY-3C-derived ICPs and digisonde-derived ones should be mainly attributed to the possible factors that might affect the quality of FY-3C RO products, among which the error introduced by the assumption of ionospheric symmetry used in the Abel inversion method was unnegligible.

Table 2. The statistical parameters for the comparisons of ICPs derived by FY-3C RO and other observations.

Collocation Criteria	FY-3C RO and COSMIC RO		FY-3C RO and Digisonde
	(3°, 5°, 1 h)	(3°, 5°, 1 h) and DAOP ≤ 20°	(3°, 5°, 1 h)
Number of Pairs	2661	935	6576
CC of NmF2	0.952	0.965	0.924
MAB of NmF2 (10 ⁵ el/cm ³)	−0.052	−0.069	0.100
MRB of NmF2 (%)	1.201	0.337	4.102
SDAB of NmF2 (10 ⁵ el/cm ³)	1.265	1.175	1.218
SDRB of NmF2 (%)	20.218	16.515	25.065
CC of hmF2	0.902	0.916	0.832
MAB of hmF2 (km)	−0.687	0.336	2.734
MRB of hmF2 (%)	−0.102	0.217	1.515
SDAB of hmF2 (km)	23.047	22.437	26.931
SDRB of NmF2 (%)	8.172	7.539	9.910

Table 2 also shows that the consistency between the ICPs derived from the two RO missions was improved under the collocation criteria with the constraint on DAOP compared with the one without this constraint. This should be due to that when there was no constraint on DAOP in the collocation criteria, the errors in the ICPs of a collocated FY-3C RO and COSMIC RO data pair introduced by the assumption of ionospheric symmetry used in Abel inversion may differ significantly from each other, and this will bring inconsistency between the two collocated ICPs. While when the constraint on DAOP was set in the collocation criteria, the corresponding comparison results demonstrated the

inherent quality differences between the two RO missions after removing the impacts of the errors introduced by the assumption of ionospheric symmetry used in the Abel inversion method.

To further investigate the performance of FY-3C RO in different years, the comparisons of the ICPs derived from FY-3C RO with those derived from other observations (COSMIC RO or digisonde) during each year of the period 2014–2017 are presented in Figure 8. What needs to be mentioned is that to understand the inherent quality differences between the FY-3C RO-derived ionospheric products and COSMIC RO-derived ones during each year, the constraint on DAOP was set for the collocation of the ICPs from the two RO missions here. The biases (Figure 8a–d), the correlation coefficients (Figure 8e,f), and the number of matched couples (Figure 8g) between FY-3C RO-derived ICPs and the ICPs from other observations during each year are presented in this figure. In each subfigure, the blue and the pink symbols represent the comparison results between FY-3C RO and COSMIC RO, and those between FY-3C RO and digisonde observations, respectively. In the subfigures (Figure 8a–d), the points and error bars represent the means and the standard deviations of the absolute and relative biases of NmF2 (Figure 8a,b) and hmF2 (Figure 8c,d), respectively. In the subfigures (Figure 8e,f), the columns represent the correlation coefficients of NmF2 (Figure 8e) and hmF2 (Figure 8f). While in the subfigure (Figure 8g), the dotted lines represent the variations of the numbers of matched pairs during different years.

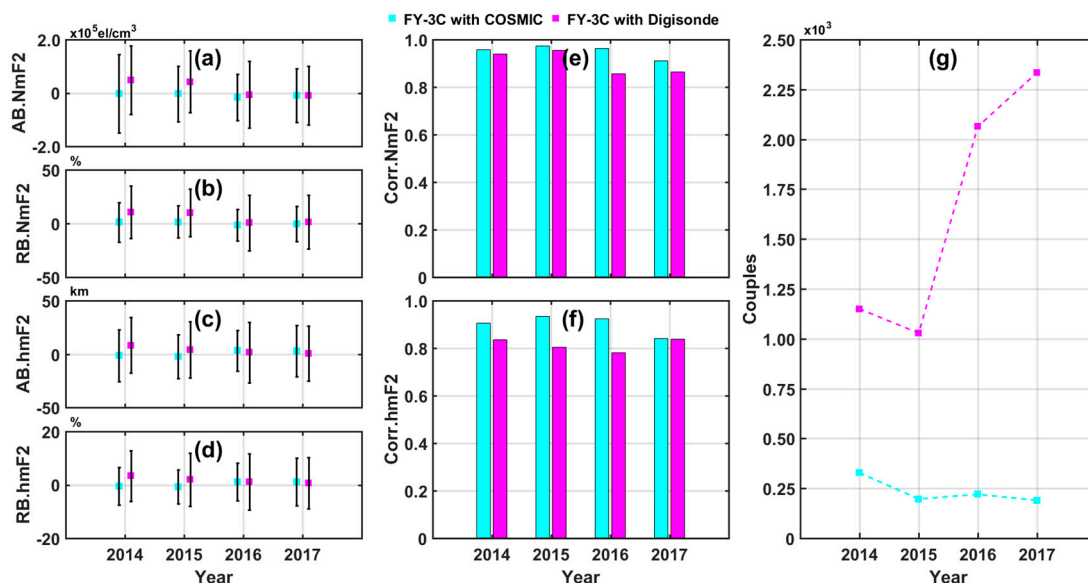


Figure 8. The comparison between FY-3C RO-derived ICPs and ICPs from other observations (COSMIC RO and digisonde) for each year during 2014–2017 for (a) ABs of NmF2, (b) RBs of NmF2, (c) ABs of hmF2, (d) RBs of hmF2, (e) CCs of NmF2, (f) CCs of hmF2 and (g) the number of the couples.

It could be seen that in every year, high correlations existed between FY-3C-derived IPPs and COSMIC-derived (digisonde-derived) ones, while the absolute and the relative biases of FY-3C RO-derived IPPs were generally low compared with the other two data sources. In each year, the correlations of NmF2, which are shown in Figure 8e, were generally higher than those of hmF2, which are shown in Figure 8f, while no matter for NmF2 or for hmF2, the agreements between FY-3C RO and COSMIC RO, which are shown by blue columns, were generally better than those between FY-3C RO and digisonde observations, which are shown by pink columns. This is because the constraint on DAOP was set for the collocation of the ICPs from the two RO missions, and the impact of the errors introduced by the assumption of ionospheric symmetry used in the Abel inversion method had been removed to a large extent from the comparison results of the two RO missions. While for the comparison of FY-3C RO and digisonde observations, this error source was negligible. For each year, all the statistical comparison parameters, including CC, MAB, MRB, SDAB, and SDRB, indicated that

good consistence existed between the ICPs derived from FY-3C RO and those derived from COSMIC RO, which proves that the ICPs derived from the two RO missions were of similar quality.

As shown in Figure 8g, the number of matched pairs between FY-3C RO and digisonde observations during 2016–2017 was significantly larger than that during 2014–2015. It should be due to the increase in the number of qualified FY-3C-derived ICPs during 2016–2017, as shown by Figure 2, allowing more qualified FY-3C-derived ICPs to be matched with digisonde observations. In addition, a close look at Figure 8a–d reveals that the biases (MAB, MRB, SDAB, SDRB) of the ICPs derived from FY-3C RO compared with those derived from digisonde observations during 2014–2015 (the higher solar activity period) were significantly larger than those during 2016–2017 (the lower solar activity period). Since digisonde observations were generally of high accuracy, the qualities of RO-derived ICPs could be presented by their biases compared with those derived from digisondes. Therefore, the comparison results of these two periods (2014–2015 and 2016–2017) will be analyzed further separately in the next section.

3.2. The Variation of the Quality of FY-3C RO-Derived ICPs with SEAs and AOPs in Different Solar Activity Periods

From the previous section, it was clear that the quality of FY-3C RO ICPs varied in different solar activity periods. During either of the two solar activity periods, the impact of solar activity on the status of the ionosphere and quality of ionospheric observations will further vary with the variation of the space and time of the observations, which are usually presented in previous studies by the variations of three impactor factors, including the latitude zone [19,29], the season [31,41], and the local time [30,31] of the observations. The integrated variation of these three factors can be presented by the variation of SEA, which was calculated by the latitude, longitude, and UTC of the observation. To be specific, for each occultation event, the SEA was calculated by the time and location corresponding to the peak electron density in the EDPs. The valid value of SEA varied from -90° to 90° , but only the non-negative value were used in the following analysis because it is unnecessary to discuss the influence of solar activity during the night. In addition to SEA, the AOP also influences the quality of the RO-derived ionospheric products [23,24].

To understand the variation of the quality of FY-3C RO-derived ICPs with the variation of SEAs and AOPs, the comparisons between FY-3C RO-derived ICPs with digisonde-derived ones are carried out for different SEA intervals and AOP intervals during the two different solar activity periods. What needs to be mentioned is that only digisonde-derived ICPs were taken as independent references in this comparison due to that they were of high quality and were not affected by the errors introduced by the RO inversion method.

According to the temporal variation of F10.7 index shown in Figure 1, the whole time period was divided into the higher solar activity period, 2014–2015, and the lower solar activity period, 2016–2017. In either of the two solar activity periods, the matched RO-derived and digisonde-derived data pairs were further classified into five groups according to the SEAs calculated by the time and locations of the RO events, which corresponded to the five SEA intervals, $[0^\circ, 18^\circ]$, $[18^\circ, 36^\circ]$, $[36^\circ, 54^\circ]$, $[54^\circ, 72^\circ]$ and $[72^\circ, 90^\circ]$. The variations of the four statistical comparison parameters, i.e., MAB, MRB, SDAB, and SDRB, with the variations of SEAs during the two different solar activity periods are shown in Figure 9a–d. Likewise, all the matched pairs are divided into nine AOP intervals by a step of 20° from 0° to 180° , and the variations of the four statistical comparison parameters with the variations of AOPs during the two different solar activity periods are presented in Figure 9e–h.

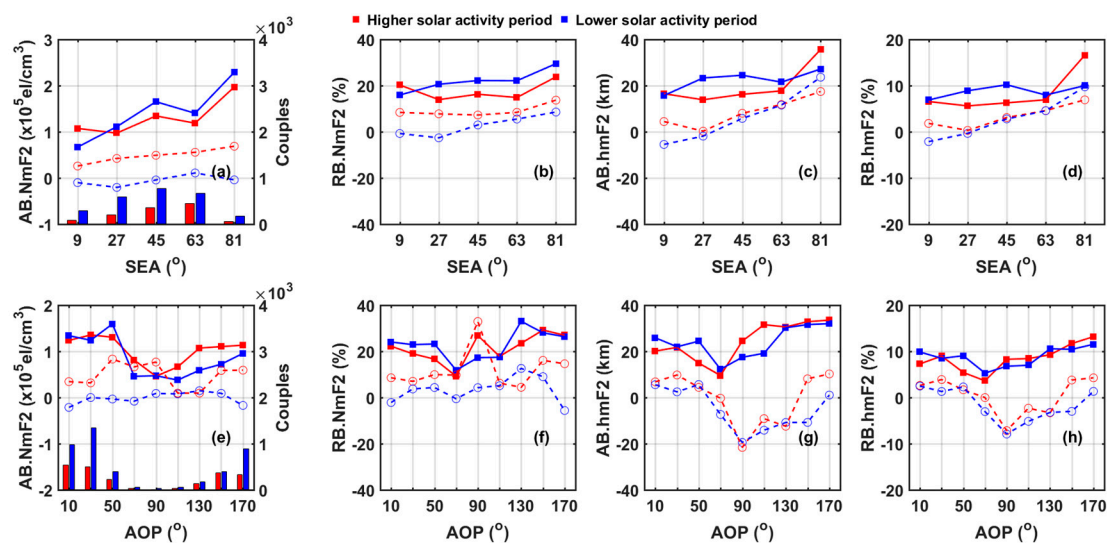


Figure 9. The variations of the standard deviation of the absolute bias (SDAB), standard deviation of the relative bias (SDRB), mean absolute bias (MAB), and mean relative bias (MRB) with the variations of (a–d) SEAs and the variations of (e–h) AOPs for the comparison between FY-3C RO-derived ICPs and the ICPs derived from digisondes.

In each subfigure of Figure 9, the red and blue symbols represent the comparison results during the higher solar activity period and the lower solar activity period, respectively. Each filled square represents the SDAB (Figure 9a,c,e,g) or the SDRB (Figure 9b,d,f,h) of the RO-derived NmF2 (Figure 9a,b,e,f) and the RO-derived hmF2 (Figure 9c,d,g,h) for the specified interval of SEA (Figure 9a–d) or AOP (Figure 9d–h), while each hollow circle represents the MAB (Figure 9a,c,e,g) or the MRB (Figure 9b,d,f,h) of the RO-derived NmF2 (Figure 9a,b,e,f) and the RO-derived hmF2 (Figure 9c,d,g,h) for the specified interval of SEA (Figure 9a–d) or AOP (Figure 9d–h). In the subfigures (Figure 9a,e), the columns (label at the right) represent the numbers of matched pairs in the corresponding ranges of SEA or AOP and the midpoints of SEA or AOP intervals are labeled on the x-axis.

Figure 9a,b demonstrate that during either of the two solar activity periods, the MAB and MRB of RO-derived ICPs were positively correlated with SEA, specifically, larger bias values of FY-3C RO derived ICPs were obtained corresponding to higher SEAs. It is noteworthy that for a certain SEA interval, the MAB and MRB of the FY-3C RO-derived ICPs were generally larger in higher solar activity period than in lower solar activity period, which indicates that the quality of FY-3C RO-derived ICPs was generally worse during high solar activity period than during low solar activity period, as shown in Figure 8a–d. Meanwhile, the SDAB and SDRB of FY-3C RO-derived ICPs compared with the digisonde-derived ones also generally increased with the increase of the SEA of the RO events. Considering that the values of standard deviations present the errors of FY-3C RO ICPs, we further calculated the rate of change (ROC) of the SDAB and SDRB with the variations in the SEAs, and ROC here was defined as the slope of the regression line of SDAB or SDRB with respect to SEA intervals. The specific values of these ROC values are listed in Table 3, which demonstrates that the ROCs of the two statistical comparison parameters were all positive.

Table 3. The rate of change (ROC) of SDABs and SDRBs with the variations of SEAs for the comparison between FY-3C RO-derived ICPs and the digisondes-derived ones.

	ROC of			
	SDAB.NmF2 ($\times 10^5$ el/cm 3 /°)	SDRB.NmF2 (%/°)	SDAB.hmF2 (km/°)	SDRB.hmF2 (%/°)
Higher solar activity period	0.806	0.305	0.752	0.734
Lower solar activity period	0.921	0.930	0.779	0.604

Figure 9e–h shows that the minimum values of SDAB and SDRB of FY-3C RO-derived ICPs were all concentrated in the AOP range of 60° – 120° , which is consistent with the results of Shaikh's simulation study [24]. It is suggested that the spherical symmetry hypothesis should have the least influence on the RO inversion results in this AOP range. However, the corresponding MAB and MRB for this AOP interval were generally larger than those for other AOP intervals.

The distributions of the numbers of FY-3C RO and digisondes matched ICPs for different SEA and AOP intervals are presented in Figure 9a,e, respectively. For all the SEA or AOP intervals, the numbers of valid matched pairs during the lower solar activity period (2016–2017) were larger than those during the higher solar activity period (2014–2015), which should be due to the increase in the number of qualified FY-3C-derived ICPs during 2016–2017, as shown by Figure 2, allowing more qualified FY-3C-derived ICPs to be matched with digisonde observations. The principle for the connection between the quality of FY-3C RO-derived ICPs and SEA will be further discussed in Section 4.

4. Discussion

In this section, we intend to make an explanation on the connection between the variation of SEA and the integrated variations of latitude, season, and local time of the observation and why the error level of RO-derived ICPs compared with digisonde measurements generally increased with the increase of SEAs. In addition, we also took into consideration the influence of AOPs on the quality of FY-3C RO-derived ICPs.

Many previous studies have demonstrated that the primary error of RO-derived EDPs comes from the horizontal gradient of electron density, which exists in the ionosphere due to the spherical symmetry assumption of the refractive index in the inversion process [23–25]. The larger the horizontal gradient of electron density, the greater the errors of RO-derived EDPs and the corresponding biases of RO-derived ICPs compared with digisonde-derived ones. Although the difference in the time and locations of RO and digisonde observations in each collocated match may also have influences on the biases of RO-derived ionospheric parameters, the influence was not taken into account in this work considering that the digisondes are distributed globally and to use the mean biases of RO-derived ICPs with reference to digisonde observations to represent the quality of the RO products is reasonable [46].

Meanwhile, the distribution of electron density mainly depends on the ionospheric behavior, specifically, the generation and movement of the ionospheric plasma, which is affected by solar, geomagnetic, and meteorology activities [47]. Since the observations when the Ap index is larger than 12 are eliminated in the process of quality control and the influence of meteorology on ionosphere mainly occurs in particular regions or periods, such as when the neutral winds cross the equator in winter [48], solar activity becomes the main factor that has impacts on the ionization of particles in global ionosphere. With the increase of solar activity, the horizontal gradient of electron density may increase correspondingly because the global distribution of ionizable particles is uneven and the regional enhancement of ionization makes the difference of ionized particles between different regions become more significant. It has been proven that the quality of ionospheric products derived from RO is generally worse in higher solar activity periods than in lower solar activity periods [29–32].

During a certain solar activity period, whether during the higher solar activity period or the lower solar activity period, it is reasonable to assume that the intensity of the solar activity is roughly stable in this period, but the distribution of the solar radiation energy around the globe and throughout the period is not uniform, which leads to a difference in the quality of the RO-derived EDPs at different times and locations. This difference of solar radiation energy during the same solar activity period can be measured by the SEA of the RO observation. Furthermore, SEA is essentially connected with the three factors, including latitude, season, and local time, which are usually taken into consideration when evaluating the quality of RO-derived EDPs. To be specific, the average annual solar radiation intensity gradually increases from a high-latitude to low-latitude region [19], while different seasons, including summer, equinox, and winter, correspond to strong, moderate, and weak monthly solar radiation respectively [45]. Solar radiation intensity also varies in different local time intervals,

including daytime, twilight, and night [28]. Therefore, all these three impact factors that are usually used, in essence, reflect the intensity of solar radiation, while the calculation of any one of these factors only depends on partial knowledge of the space and time of a RO event. For example, to know what season it is when a RO event occurs, only the information about the UTC when and the hemisphere where the event occurs is needed, while to know the local time of a RO event, only the longitude where the event occurs is needed. In comparison, the SEA is calculated using the complete information of the space and time of a RO event.

For the quality of RO-derived ionospheric parameters, the pattern of its variation with SEAs shown in Section 3 is consistent with the pattern of its variation with the three traditionally used factors, as shown in previous studies. For example, it was found that the quality of RO-derived ICPs is worse in a low-latitude area than in a mid-latitude area during one year [19,32], which can be explained by the high values of SEAs (near 90°) in low latitudes considering that the point of direct sunlight moves between the tropic of Cancer and the tropic of Capricorn throughout the year. Huang et al. [45] found that the quality of RO-derived ICPs is better in the equinox seasons than in the summer seasons during the period of 2007–2013 over the equator, which can also be explained by that for a certain region, the SEAs are generally higher in summer than in the equinox seasons.

It is noteworthy that even for the same level of solar activity, significant differences may exist in the horizontal gradients of electron densities for ray paths along different directions. In general, the ray path along the latitude direction, which means the direction corresponding to the AOP of around 0° or 180° , experiences a larger horizontal gradient of electron densities than the ray path along the longitude direction, which means the direction corresponding to the AOP of around 90° . It should be the reason why the SDAB and SDRB of the FY-3C RO-derived ICPs generally reach the minimum values for the AOP interval of 60° – 120° , as shown by Figure 9e–h. Based on a simulation, Shaikh et al. [24] indicates that the RO EDPs corresponding to AOPs of 80° – 100° might be of the least errors introduced by the spherical symmetry assumption applied in Abel inversion in general. Our analyses about the ICPs derived by FY-3C RO mission were consistent with Shaikh et al. [24] to some extent. What needs to be mentioned is that for some abnormal areas such as the areas of equatorial ionization anomaly (EIA), the variation of the quality of RO-derived ICPs with AOPs may be different from the aforementioned general pattern. This is due to that it is very likely that the electron density gradient is greater along the longitude direction than that along the latitude direction over these areas.

5. Conclusions

In this paper, the ICPs derived from FY-3C RO during 2014 to 2017 are compared with those derived from COSMIC RO and from the observations of 24 globally distributed digisonde stations. When comparing the ICPs derived from the two RO missions, the DAOP between the matched pairs is limited to be within 20° . The correlation and bias analyses are carried out in the comparison. SEA is used as an integrated factor whose variation reflects the integrated variations of latitude zones, seasons, and local time. The variation of the biases and standard deviations of FY-3C RO-derived ICPs with SEAs and AOPs in the two different solar activity periods, i.e., the higher solar activity period, 2014–2015, and the lower solar activity period, 2016–2017, were analyzed. The results are shown as follows:

- (1) There was good agreement between the ICPs derived from FY-3C RO and those provided by other observations (COSMIC RO and digisonde). Specifically, the CC (MAB and MRB) of the ICPs derived from FY-3C RO and those from other observations were all of high (low) values in each year from 2014 to 2017 and for the whole time period. It is convincing that the ionospheric products provided by FY-3C RO were reliable enough for further ionospheric and geophysical applications.
- (2) The CC of NmF2 was, in general, higher than that of hmF2 when comparing FY-3C RO with other observations, and the MAB and MRB of FY-3C RO-derived ICPs compared with other observations were generally higher during the higher solar activity period than those during the

low solar activity period. It is noteworthy that the differences between the two RO missions were smaller than the differences between FY-3C RO and digisondes.

- (3) The AOP plays an essential role in the quality analysis of RO-derived ICPs. It was found that, in general, the SDAB and SDRB of RO-derived ICPs both get the minimum values when the AOP was near to 90° , specifically, for the AOP interval of $[60^\circ, 120^\circ]$.
- (4) In a certain solar activity period, the SDAB and SDRB of RO-derived ICPs compared with the digisonde-derived ICPs generally increased with the increase of SEA, and the quality of RO-derived ICPs was the worst when SEA reached the maximum. When analyzing the quality of the ionospheric products derived from RO, it is meaningful to use SEA as a new impact factor, which reflects the integrated influence of the three traditionally used factors including latitude, season, and local time.

Author Contributions: J.L. and X.X. conceptualized the initial idea and experiment design; H.W. analyzed the data; H.W., J.L. and X.X. wrote the main manuscript text; J.L. reviewed and edited the paper.

Funding: This research was funded by the National Natural Science Foundation of China (Grant No. 41774032 and 41774033), the National Key Research and Development Program of China (Grant No. 2018YFC1503502), and the National Basic Research Program of China (973 Program) (Grant No. 2013CB733302).

Conflicts of Interest: The authors declare no conflict of interests.

References

1. Kursinski, E.R.; Hajj, G.A.; Schofield, J.T.; Linfield, R.P. Observing Earth's atmosphere with radio occultation measurements using the global positioning system. *J. Geophys. Res. Biogeosci.* **1997**, *102*, 23429–23465. [[CrossRef](#)]
2. Hajj, G.A.; Kursinski, E.R.; Romans, L.J.; Bertiger, W.I.; Leroy, S.S. Technical description of atmospheric sounding by GPS occultation. *J. Atmos. Sol. Terr. Phys.* **2002**, *64*, 451–469. [[CrossRef](#)]
3. Anthes, R.A. Exploring Earth's atmosphere with radio occultation: Contributions to weather, climate and space weather. *Atmos. Meas. Tech.* **2011**, *4*, 1077–1103. [[CrossRef](#)]
4. Hajj, G.A.; Romans, L.J. Ionospheric electron density profiles obtained with the Global Positioning System: Results from the GPS/MET experiment. *Radio Sci.* **1998**, *33*, 175–190. [[CrossRef](#)]
5. Schreiner, W.S.; Sokolovskiy, S.V.; Rocken, C.; Hunt, D.C. Analysis and validation of GPS/MET radio occultation data in the ionosphere. *Radio Sci.* **1999**, *34*, 949–966. [[CrossRef](#)]
6. Yue, X.; Schreiner, W.S.; Pedatella, N.; Anthes, R.A.; Mannucci, A.J.; Straus, P.R.; Liu, J.Y. Space Weather Observations by GNSS Radio Occultation: From FORMOSAT-3/COSMIC to FORMOSAT-7/COSMIC-2. *Space Weather* **2014**, *12*, 616–621. [[CrossRef](#)]
7. Wickert, J.; Reigber, C.; Beyerle, G.; König, R.; Marquardt, C.; Schmidt, T.; Grunwaldt, L.; Galas, R.; Meehan, T.K.; Melbourne, W.G.; et al. Atmosphere sounding by GPS radio occultation: First results from CHAMP. *Geophys. Res. Lett.* **2001**, *28*, 3263–3266. [[CrossRef](#)]
8. Beyerle, G.; Wickert, J.; Schmidt, T.; Reigber, C. GPS radio occultation with GRACE: Atmospheric profiling utilizing the zero difference technique. *Geophys. Res. Lett.* **2005**, *32*, L13806. [[CrossRef](#)]
9. Anthes, R.A.; Ector, D.; Hunt, D.C.; Kuo, Y.-H.; Rocken, C.; Schreiner, W.S.; Sokolovskiy, V.S.; Syndergaard, S.; Wee, T.K.; Zeng, Z. The COSMIC/FORMOSAT-3 mission: Early results. *Bull. Am. Meteorol. Soc.* **2008**, *89*, 313–333. [[CrossRef](#)]
10. Rapp, M.; Dörnbrack, A.; Kaifler, B. An intercomparison of stratospheric gravity wave potential energy densities from METOP GPS radio occultation measurements and ECMWF model data. *Atmos. Meas. Tech.* **2018**, *11*, 1031–1048. [[CrossRef](#)]
11. Bi, Y.; Yang, Z.; Zhang, P.; Sun, Y.; Bai, W.; Du, Q.; Yang, G.; Chen, J.; Liao, M. An introduction to China FY3 radio occultation mission and its measurement simulation. *Adv. Space Res.* **2012**, *49*, 1191–1197. [[CrossRef](#)]
12. Mao, T.; Sun, L.; Yang, G.; Yue, X.; Yu, T.; Huang, C.; Zeng, Z.; Wang, Y.; Wang, J. First Ionospheric Radio-Occultation Measurements From GNSS Occultation Sounder on the Chinese Feng-Yun 3C Satellite. *IEEE Trans. Geosci. Remote Sens.* **2016**, *54*, 5044–5053. [[CrossRef](#)]

13. Brahmanandam, P.S.; Uma, G.; Liu, J.Y.; Chu, Y.H.; Latha Devi, N.S.M.P.; Kakinami, Y. Global S4 index variations observed using FORMOSAT-3/COSMIC GPS RO technique during a solar minimum year. *J. Geophys. Res.* **2012**, *117*, A09322. [[CrossRef](#)]
14. Straus, P. Ionospheric climatology derived from gps occultation observations made by the ionospheric occultation experiment. *GPS Solut.* **2005**, *9*, 164–173. [[CrossRef](#)]
15. Arras, C.; Wickert, J.; Jacobi, C.; Heise, S.; Beyerle, G.; Schmidt, T. A global climatology of ionospheric irregularities derived from GPS radio occultation. *Geophys. Res. Lett.* **2008**, *35*, L14809. [[CrossRef](#)]
16. Watson, C.; Pedatella, N.M. Climatology and characteristics of medium-scale F region ionospheric plasma irregularities observed by COSMIC radio occultation receivers. *J. Geophys. Res. Space Phys.* **2018**, *123*, 8610–8630. [[CrossRef](#)]
17. Bai, W.H.; Sun, Y.Q.; Du, Q.F.; Yang, G.L.; Yang, Z.D.; Zhang, P.; Bi, Y.M.; Wang, X.Y.; Cheng, C.; Han, Y. An introduction to the FY3 GNOS instrument and mountain-top tests. *Atmos. Meas. Tech.* **2014**, *7*, 1817–1823. [[CrossRef](#)]
18. Zeng, T.; Sui, L.F.; Jia, X.L. Results and Analysis of BDS Precise Orbit Determination with the Enhancement of Fengyun-3C. *Acta Geod. Cartogr. Sin.* **2017**, *59*, 419–425.
19. Yang, G.L.; Sun, Y.Q.; Bai, W.H.; Zhang, X.X.; Liu, C.L.; Meng, X.G.; Bi, Y.M.; Wang, D.W.; Zhao, D.Y. Validation results of NmF2 and hmF2 derived from ionospheric density profiles of GNOS on FY-3C satellite. *Sci. China Technol. Sci.* **2018**, *61*, 1372–1383. [[CrossRef](#)]
20. Huang, X.; Reinisch, B.W. Vertical electron density profiles from the Digisonde network. *Adv. Space Res.* **1996**, *18*, 121–129. [[CrossRef](#)]
21. Reinisch, B.W.; Huang, X.; Galkin, I.A.; Paznukhov, V.; Kozlov, A. Recent advances in real-time analysis of ionograms and ionospheric drift measurements with digisondes. *J. Atmos. Sol. Terr. Phys.* **2005**, *67*, 1054–1062. [[CrossRef](#)]
22. Reinisch, B.W.; Galkin, I.A.; Khmyrov, G.M.; Kozlov, A.V.; Bibl, K.; Lisysyan, I.A.; Cheney, G.P.; Huang, X.; Kitrosser, D.F.; Paznukhov, V.V.; et al. New Digisonde for research and monitoring applications. *Radio Sci.* **2009**, *44*, RS0A24. [[CrossRef](#)]
23. Yue, X.A.; Schreiner, W.S.; Lei, J.H.; Sokolovskiy, S.V.; Rocken, C.; Hunt, D.C.; Kuo, Y.H. Error analysis of Abel retrieved electron density profiles from radio occultation measurements. *Ann. Geophys.* **2010**, *28*, 217–222. [[CrossRef](#)]
24. Shaikh, M.; Notarpietro, R.; Nava, B. The impact of spherical symmetry assumption on radio occultation data inversion in the ionosphere: An assessment study. *Adv. Space Res.* **2014**, *53*, 599–608. [[CrossRef](#)]
25. Pedatella, N.M.; Yue, X.; Schreiner, W.S. An improved inversion for FORMOSAT-3/COSMIC ionosphere electron density profiles. *J. Geophys. Res. Space Phys.* **2015**, *120*, 8942–8953. [[CrossRef](#)]
26. Yang, J.J.; Huang, J.; Xu, J.; Deng, B.C.; Quan, H.J. Study of Sporadic E Layers Based on Occultation Data Observed by FY-3C Satellite. *Space Sci.* **2016**, *36*, 305–311. (In Chinese)
27. Reinisch, B.W.; Cooke, D.L.; McNamara, L.F.; Valladares, C.E. Comparison of CHAMP and Digisonde plasma frequencies at Jicamarca, Peru. *Radio Sci.* **2007**, *42*, RS2005.1–RS2005.14.
28. Chu, Y.H.; Su, C.L.; Ko, H.T. A global survey of COSMIC ionospheric peak electron density and its height: A comparison with ground-based ionosonde measurements. *Adv. Space Res.* **2010**, *46*, 431–439. [[CrossRef](#)]
29. Ely, C.V.; Batista, I.S.; Abdu, M.A. Radio occultation electron density profiles from the FORMOSAT-3/COSMIC satellites over the Brazilian region: A comparison with Digisonde data. *Adv. Space Res.* **2012**, *49*, 1553–1562. [[CrossRef](#)]
30. Hu, L.; Ning, B.; Liu, L.; Zhao, B.; Li, G.; Wu, B.; Huang, Z.; Hao, X.; Chang, S.; Wu, Z. Validation of COSMIC ionospheric peak parameters by the measurements of an ionosonde chain in China. *Ann. Geophys.* **2014**, *32*, 1311–1319. [[CrossRef](#)]
31. Luo, J.; Sun, F.F.; Xu, X.H.; Wang, H. Ionospheric F2-Layer critical frequency retrieved from COSMIC radio occultation: A statistical comparison with measurements from a meridional ionosonde chain over Southeast Asia. *Adv. Space Res.* **2019**, *63*, 327–336. [[CrossRef](#)]
32. Wu, X.; Hu, X.; Gong, X.; Zhang, X.; Wang, X. Analysis of inversion errors of ionospheric radio occultation. *GPS Solut.* **2009**, *13*, 231–239. [[CrossRef](#)]
33. Hernandez-Pajares, M.; Juan, J.M.; Sanz, J. Improving the Abel inversion by adding ground GPS data to LEO radio occultations in ionospheric sounding. *Geophys. Res. Lett.* **2000**, *27*, 2473–2476. [[CrossRef](#)]

34. Garcia-Fernandez, M.; Hernandez-Pajares, M.; Juan, J.M.; Sanz, J. Improvement of ionospheric electron density estimation with GPSMET occultations using Abel inversion and VTEC information. *J. Geophys. Res.* **2003**, *108*, 1338. [CrossRef]
35. Garcia-Fernandez, M.; Hernandez-Pajares, M.; Juan, J.M.; Sanz, J. Performance of the improved Abel transform to estimate electron density profiles from GPS Occultation data. *GPS Solut.* **2005**, *9*, 105–110. [CrossRef]
36. Lei, J.H.; Syndergaard, S.; Burns, A.G.; Solomon, S.C.; Wang, W.B.; Zeng, Z.; Roble, R.G.; Wu, Q.; Kuo, Y.H.; Holt, J.M.; et al. Comparison of COSMIC ionospheric measurements with ground-based observations and model predictions: Preliminary results. *J. Geophys. Res.* **2007**, *112*, A07308. [CrossRef]
37. Yang, K.F.; Chu, Y.H.; Su, C.L.; Ko, H.T.; Wang, C.Y. An examination of FORMOSAT-3/COSMIC ionospheric electron density profile: Data quality criteria and comparisons with the IRI model. *Terr. Atmos. Ocean. Sci.* **2009**, *20*, 193–206. [CrossRef]
38. Uma, G.; Brahmanandam, P.S.; Chu, Y.H. A long-term study on the deletion criterion of questionable electron density profiles caused by ionospheric irregularities-COSMIC radio occultation technique. *J. Space Res.* **2016**, *57*, 2452–2463. [CrossRef]
39. Guo, P.; Xu, X.; Zhang, G.X. Analysis of the ionospheric equivalent slab thickness based on ground-based GPS-TEC and GPS/COSMIC RO measurement. *J. Atmos. Sol.-Terr. Phys.* **2011**, *73*, 839–846. [CrossRef]
40. Luo, J.; Wang, H.; Xu, X.; Sun, F.F. The influence of the spatial and temporal collocation windows on the comparisons of the ionospheric characteristic parameters derived from COSMIC Radio Occultation and Digisondes. *Adv. Space Res.* **2019**, *63*, 3088–3101. [CrossRef]
41. Kumar, S.; Singh, R.P.; Tan, E.L.; Singh, A.K.; Ghodpage, R.N.; Siingh, D. Temporal and spatial deviation in F-2 peak parameters derived from FORMOSAT-3/COSMIC. *Space Weather* **2016**, *14*, 391–405. [CrossRef]
42. Galkin, I.A.; Reinisch, B.W.; Huang, X.; Khmyrov, G.M. Confidence score of ARTIST-5 ionogram autoscaling. In *INAG Technical Memorandum*; 25 November 2013; pp. 1–7. Available online: http://www.ursi.org/files/CommissionWebsites/INAG/web-73/confidence_score.pdf (accessed on 1 March 2014).
43. McNamara, L.F.; Thompson, D.C. Validation of COSMIC values of foF2 and M(3000)F2 using ground-based ionosondes. *Adv. Space Res.* **2015**, *55*, 163–169. [CrossRef]
44. McNamara, L.F.; Wilkinson, P.J. Spatial correlations of foF2 deviations and their implications for global ionospheric models: 1. Ionosondes in Australia and Papua New Guinea. *Radio Sci.* **2009**, *44*, RS2016. [CrossRef]
45. Huang, Z.; Yuan, H. An analysis of ionospheric characteristic parameters retrieved from COSMIC and IRI at Jicamarca during the period of 2007–2013. *Chin. J. Geophys.* **2016**, *59*, 2333–2343. (In Chinese)
46. Sun, B.; Reale, A.; Seidel, D.J.; Hunt, D.C. Comparing radiosonde and COSMIC atmospheric profile data to quantify differences among radiosonde types and the effects of imperfect collocation on comparison statistics. *J. Geophys. Res.* **2010**, *115*, D23104. [CrossRef]
47. Xu, G.R.; Wan, W.X.; Ning, B.Q. Applying partial correlation method to analyzing the correlation between ionospheric NmF2 and height of isobaric level in the lower atmosphere. *Chin. Sci. Bull.* **2007**, *52*, 2413–2419. [CrossRef]
48. Sun, L.F.; Zhao, B.Q.; Yue, X.A.; Mao, T. Comparison between ionospheric character parameters retrieved from FORMOSAT3 measurement and ionosonde observation over China. *Chin. J. Geophys.* **2014**, *57*, 3625–3632. (In Chinese)

